Abdominal Radiology (2019) 44:3175–3184
https://doi.org/10.1007/s00261-019-02104-1

PELVIS

Texture analysis of placental MRI: can it aid in the prenatal diagnosis of placenta accreta spectrum?

Eric Chen[1] · Winnie A. Mar[2] · Jeanne M. Horowitz[3] · Amanda Allen[2] · Priyanka Jha[4] · Donald R. Cantrell[3] · Kejia Cai[2]

Published online: 25 June 2019

Abstract

Purpose To determine if texture analysis can differentiate placenta accreta spectrum (PAS) from normal placenta on MRI.

Methods We performed retrospective image analysis of 80 patients, comprised of 46 patients with PAS and 34 patients without PAS. Histopathology was used as the reference standard. Sagittal single shot fast spin echo T2-weighted MRI sequences acquired from a single institution were analyzed. Placental heterogeneity was quantified using in-house software on a Matlab platform, including the standard deviation of pixel intensity, coefficient of variation, gray-level co-occurrence matrices (GLCM), histogram-oriented gradients (HOG), and fractal analysis with box sizes from 2 to 512. Two-tailed unpaired Student's t test was used with statistical significance of $p < 0.05$.

Results PAS was associated with higher values for standard deviation of pixel intensity and fractal analysis at every box size. Fractal analysis at box sizes 256 ($p = 0.011$) and 32 ($p = 0.021$), and standard deviation of pixel intensity ($p = 0.023$) were the most statistically significant. Fractal values at box size 256 for PAS was 0.13 versus 0.090 for patients without PAS, while standard deviation of pixel intensity was 3.7 for PAS versus 2.5 for patients without PAS. No statistically significant association between PAS and GLCM, coefficient of variation, and HOG was found.

Conclusion Statistically significant differences were found between normal and abnormal groups using standard deviation of pixel intensity and fractal analysis.

Keywords Placenta accreta spectrum · Placenta accreta · Texture analysis · Fractal analysis · MRI

Introduction

Placenta accreta spectrum (PAS) encompasses different levels of abnormal placental invasion including placenta accreta vera, increta, and percreta, and occurs due to a defect in the decidua basalis. PAS is the preferred terminology determined by the recent 2018 Federation of International Gynecologists and Obstetricians (FIGO) consensus statement [1]. The potential outcomes can be devastating, including severe maternal hemorrhage and death, with mortality reported as high as 6–7% [2, 3]. Overall, the incidence of PAS has been steadily increasing, concordant with the increasing rate of cesarean sections (C-sections) [4]. Ultrasound is the first imaging examination where PAS is suspected. Although there are differences in opinion over

✉ Winnie A. Mar
wmar@uic.edu

Eric Chen
elchen2@uic.edu

Jeanne M. Horowitz
jhorowit@nmff.org

Amanda Allen
aallen33@uic.edu

Priyanka Jha
priyanka.jha@ucsf.edu

Donald R. Cantrell
Donald-cantrell@northwestern.edu

Kejia Cai
kcai@uic.edu

1 College of Medicine, University of Illinois at Chicago, 1835 W Polk St, Chicago, IL 60612, USA

2 Department of Radiology, University of Illinois at Chicago, 1740 W Taylor Street Rm 2483, (MC 931), Chicago, IL 60612, USA

3 Northwestern Memorial Hospital, 676 N St Clair St Ste 800, Chicago, IL 60611, USA

4 Department of Radiology, University of California, San Francisco, 505 Parnassus Ave, Box 0628, San Francisco, CA 94131, USA

whether MRI should be performed [5], MRI is typically recommended when ultrasound is inconclusive or topographical evaluation of suspected PAS is desired. It has been shown to be particularly helpful for posterior, lateral and cervical invasion [6, 7]. The sensitivity and specificity of MRI for PAS in a large meta-analysis of 1010 cases was 94.4 and 84.0%, respectively [7]. In a recent article, MRI has been shown to correctly upstage the diagnosis in 9% of cases, although it correctly or incorrectly altered the ultrasound diagnosis in 19 and 17%, respectively [5, 8].

Heterogeneity is an important MRI parameter to detect placenta accreta, which is currently based on a subjective assessment. There are several factors which contribute to placental heterogeneity in PAS, including the presence of dark bands and altered placental vascularity [9]. Other MRI findings of PAS include focally interrupted myometrium, lower uterine bulging, and myometrial thinning. Placenta previa is also associated with PAS in about half of cases [10]. Increasing gestational age in the late third trimester also contributes to heterogeneity resulting in overlap in imaging features of a maturing placenta and PAS. Thus, it is recommended that MRI be performed in the late second or the early third trimester [9].

Texture analysis, a part of radiomics, is a quantitative measure of heterogeneity and other imaging features beyond what is visible to the eye [11]. First-order statistics-based texture analysis such as histogram analysis, evaluates the number of pixels with a certain gray-level value. Second-order statistics-based texture analysis such as gray-level co-occurrence matrices (GLCM) also evaluates the spatial relationship of pixels with a certain gray-level value. Complex internal architectures of malignant tumors secondary to aggressive growth patterns, neovascularity and tumor necrosis can be quantified using second-order texture analysis [11]. Model-based texture analysis, such as fractal analysis, uses advanced mathematical calculations to evaluate complexity [12].

PAS remains a difficult diagnosis that is subject to inter-observer variability and reader experience. Although previous studies have evaluated texture analysis in the setting of oncologic [13, 14], neurologic [15, 16], cardiac [17], and musculoskeletal imaging [18], there is a paucity of studies about the use of texture analysis on MRI to diagnose PAS. Hence, we aim to develop an objective and quantitative measurement of placental heterogeneity based on texture analysis to differentiate between normal placenta and PAS.

Methods

This study was approved by the Institutional Review Board (IRB). MRI studies were retrospectively collected from 80 pregnant patients aged 21-45 (mean ± S.D., 35.1 ± 5.1) with gestational ages ranging from 14 to 41 weeks (mean 28.8 ± 5.8). The majority of patients had an MRI scan during the early third trimester from 29 to 35 weeks (45 patients) or late second trimester from 21 to 28 weeks (21 patients). Only six patients had an MRI scan from 36 to 41 weeks, and 11 patients were scanned at 14 to 20 weeks gestational age. These patients had MRI for suspected PAS at a single university hospital secondary to an inconclusive ultrasound, or for surgical planning in the setting of suspicious ultrasound findings.

All MRI was performed between 1/9/2008 and 10/19/2014 with a Siemens (Erlangen, Germany) Avanto, Espree or Aera 1.5 Tesla MRI. Imaging was performed using a 4 channel phased array body coil per routine protocol (Table 1) consisting of T2-weighted half-fourier acquisition single shot turbo spin echo (HASTE) and true fast imaging with steady-state free precession images (FISP) in axial, sagittal and coronal planes, axial fast spin echo T2 weighted images and axial and sagittal diffusion-weighted images with B values at 500 and 1000. Typical parameters on MRI were as follows: TR 1000, TE 64, flip angle 160, slice thickness 5, number of signal averages 1, 45 mT/m with a slew rate of 200 T/m/s and no parallel imaging. No contrast was administered. Imaging planes were performed according to the mother's body. The images obtained were stored using the Northwestern University Neuroimaging Data Archive (NUNDA) [19].

Table 1 MRI parameters

Sequence	Planes	TE (ms)	TR (ms)	FOV (cm)	Slice Thickness (mm)	Flip Angle	Bandwidth (MHz)	ETL	Matrix
T1-weighted TSE	Axial	10	684	32	6	180	182	3	320×240
T2-weighted TSE	Sagittal	79	4650	32	5	144	260	19	256×256
T2-weighted HASTE	Axial, coronal, sagittal	64	1800	34	5	160	592	256	256×160
True FISP	Axial, coronal, sagittal	1.8	411	30	5	62	1221	1	256×182
DWI (b values = 0 and 500 s/mm^2)	Axial, sagittal	78	8700	35	8	90	1447	1	182×180

TE echo time, *TR* repetition time, *FOV* field-of-view, *ETL* echo-train length, *FISP* fast imaging with steady-state precession, *TSE* turbo spin echo

Sagittal T2-weighted HASTE images were analyzed. A region of interest (ROI) including the entire placenta on all images of this sequence was manually drawn by a radiologist in training with 2 years of experience (Fig. 1). ROI placement was confirmed by an abdominal imaging fellowship trained radiologist with 15 years of experience. The time between MRI and delivery varied based on clinical factors and the time of presentation. Most of the patients with suspected PAS had a C-section at 34 weeks, and some with a lower level of suspicion were delivered at 37 weeks. Pathology specimens were reviewed per routine clinical protocol by pathologists subspecialized in placental evaluation. The pathological criteria used for accreta/increta/percreta are as follows: accreta–villous tissue (villi or perivillous fibrin) directly adjacent to myometrium without intervening decidua or trophoblast diagnosed on either a placenta or cesarean hysterectomy specimen; increta—the above criteria is used in addition to placenta infiltrating into myometrial wall; percreta–villous tissue extending to uterine serosa or adjacent structures. We defined postoperative histology to be "abnormal" if there was any degree of placental invasion, including placenta accreta vera, increta and percreta, due to the limited sample size.

To quantify tissue heterogeneity of the placenta, we utilized five commonly employed texture analyses for signal heterogeneity: histogram analysis, coefficient of variation calculation, histogram orientation gradient (HOG) analysis, GLCM and fractal dimension analysis. Customized MATLAB programs (version R2012b, MathWorks, Natick, MA) were developed for each of these algorithms. Histogram analysis is a first-order statistics-based texture analysis which is performed by fitting the pixel signal intensities of placenta with a Gaussian function, which provides the standard deviation as a variable for tissue heterogeneity. A wider range of pixel intensities indicates increased heterogeneity (Figs. 1, 2). Coefficient of variation is the ratio of standard deviation to the mean of the pixel intensity in the placental ROI. The goal is to quantify dispersion of the distribution of pixel intensities [12]. HOG evaluates occurrences of the gradient orientation in localized portions of an image. Intensity orientation captures prominent direction of intensity change [20], suggests relevant cellular activity and local entropy. GLCM represents the joint probability distribution between the grey-level values of the pairs of pixels at a predetermined distance and orientation [12]. In fractal dimension analysis, the image is called a fractal if it displays self-similarity and is split into various parts; each of which is a reduced-size copy of the whole. Our study utilized the box counting method to analyze each piece at a smaller scale with each box size as a power of two. The goal of the fractal dimension box counting method is to analyze the image by the complexity changes at different grey-level thresholds [12].

The maternal age, gestational age, method of delivery, major complications, estimated blood loss, and number

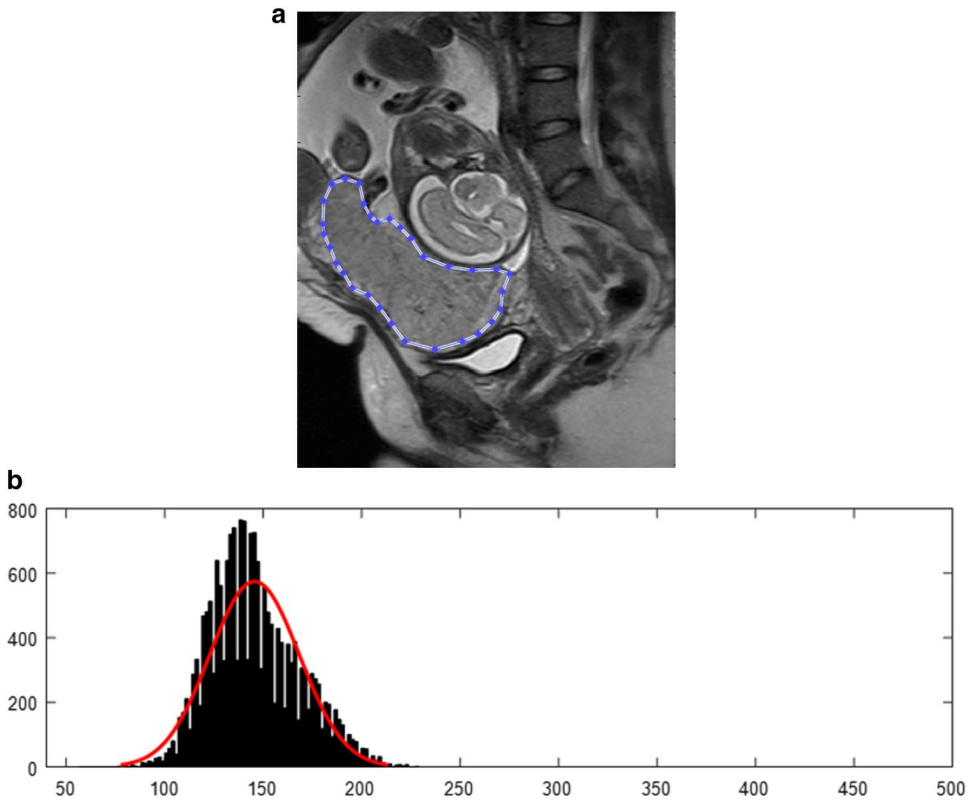

Fig. 1 A 26-year-old woman with a normal placenta. **a** Sagittal T2 MR image showing a homogeneous placenta and the method for outlining of the placenta in MATLAB. **b** Histogram from the standard deviation of pixel intensity texture analysis obtained from the placenta on this representative image shows a relatively narrow distribution of pixel intensity indicating homogeneity

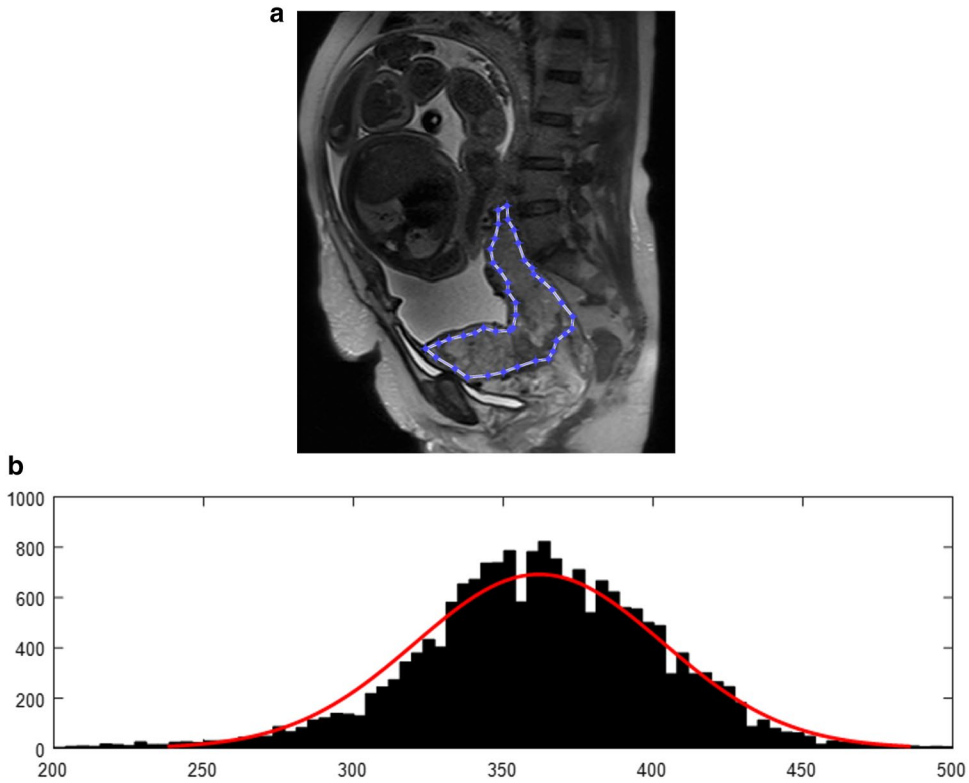

Fig. 2 A 35-year-old woman with placenta increta. **a** Sagittal T2 MR image showing a heterogeneous placenta and the method for outlining of the placenta in MATLAB. **b** The histogram from the standard deviation of pixel intensity texture analysis obtained from the placenta on this representative image shows a wider distribution of pixel intensity indicating heterogeneity

of prior C-sections were recorded for each case. Values of texture analysis variables for tissue heterogeneity were computed with our customized programs and averaged across the entire placenta.

Statistical analysis was performed using a two tail unpaired *t* test to compare between the accreta and normal groups for each variable. The level of statistical significance was set at a *p* value of 0.05. Since placental heterogeneity on T2 weighted images increases as pregnancy progresses, we performed multiple linear regression analysis and subgroup analysis (stratified analysis) to evaluate whether gestational age was a confounding variable. Stratified analysis involved separating the patients into subgroups (strata) based on gestational trimester (1st trimester, 2nd trimester, and 3rd trimester). We evaluated the association between texture analysis values and pathology (abnormal vs. normal placenta) of patients within the same strata. This allowed us to evaluate whether the magnitude and direction of this association depended on the strata, or whether our conclusions of this association differed among strata and the overall study group, whereby differences would suggest that gestational age is a confounding factor. In addition, we performed a lack-of-fit test to determine if the effect of increasing gestational age on these variables can be explained by a linear model. Quantile–quantile (Q–Q) plots plotting the residuals versus the standard normal distribution were used to check the assumption that the data was normally distributed.

Results

We reviewed 80 cases, with 34 normal and 46 abnormal cases using the pathologic diagnosis of accreta as the reference standard, as shown in Table 2. Out of our total number of subjects, 46 had an anterior placenta, 11 had a posterior placenta and 23 were located in the midline overlying the cervix. Of the abnormal cases, postoperative histologic assessment revealed 23 had accreta, 9 had increta, and 14 had percreta. Abnormal pathology was associated with a statistically significant higher amount of blood loss ($p < 0.001$), but not maternal age ($p = 0.77$), number of prior C-sections ($p = 0.25$), or gestational age ($p = 0.59$). However, when the abnormal subgroups (i.e. accreta, increta, percreta) were evaluated individually, percreta was associated with more prior C-sections compared to normal placenta ($p = 0.014$) and accreta ($p = 0.003$).

Our results included five main variables: standard deviation of pixel intensity, coefficient of variation, HOG, GLCM, and fractal analysis with box size from 2 to 512. The outcomes of t tests using these variables to differentiate between normal and abnormal placenta are shown in Table 3. Fractal analysis at box sizes 256 ($p = 0.013$) and 32 ($p = 0.021$) and standard deviation of pixel intensity ($p = 0.023$) demonstrated the most statistical significance. Fractal analysis at every box size except 512 was also statistically significant. GLCM, coefficient of variation, and HOG showed no statistically significant association with PAS at $p = 0.44$, 0.21,

Table 2 Descriptive data grouped by pathology

Mean values	Normal $n=34$	Abnormal $n=46$	Accreta $n=23$	Increta $n=9$	Percreta $n=14$
Maternal age (years)	35.3	35.0	35.5	33.4	35.1
Gestational age (weeks)	28.4	29.2	28.3	31.6	28.9
Number of prior C-sections	1.3	1.6	1.0	1.9	2.3
Blood loss (ml)	876	3720	2174	2689	6921
Incidence of complications					
Major obstetric hemorrhage[a]	0	29	11	7	11
C-hysterectomy	0	8	3	2	3
Cystotomy	0	7	0	1	6
Uterine rupture	0	2	0	0	2
Method of delivery					
NSVD	3	2	2	0	0
Abortion	5	4	3	0	1
C-section	25	8	8	0	0
C-hysterectomy	1	32	10	9	13

[a]Defined as blood loss > 1500 ml

Table 3 Results of unpaired *t* tests comparing normal versus abnormal pathology

	Normal ($n=34$)		Abnormal ($n=46$)		*p*-value
	M	SD	M	SD	
σ*	**2.5**	**1.8**	**3.7**	**2.8**	**0.0228**
CoefVariance	6.1	2.8	5.3	2.5	0.208
GLCM	0.9996	0.0005	0.9995	0.0004	0.440
HOG	18.1	7.0	16.0	7.2	0.192
df1	**286.9**	**284.3**	**434.7**	**377.1**	**0.0491**
df2	**74.9**	**72.8**	**113.1**	**96.8**	**0.0471**
df4	**20.3**	**19.1**	**30.5**	**25.5**	**0.0443**
df8	**5.9**	**5.2**	**8.7**	**7.1**	**0.0442**
df16	**1.9**	**1.5**	**2.8**	**2.1**	**0.0232**
df32	**0.70**	**0.50**	**1.0**	**0.73**	**0.0206**
df64	**0.31**	**0.18**	**0.43**	**0.30**	**0.0268**
df128	**0.17**	**0.10**	**0.23**	**0.15**	**0.0443**
df256	**0.090**	**0.050**	**0.13**	**0.094**	**0.0108**
df512	0.060	0.032	0.066	0.030	0.389

M mean, *SD* standard deviation

p-value < 0.05 considered statistically significant. Statistically significant in bold. *σ refers to standard deviation of signal intensity

and 0.19, respectively. Of the differences that were statistically significant, abnormal pathology was associated with higher values for standard deviation of pixel intensity (3.7 compared to 2.5 for normal pathology), as well as fractal analysis at every box size (Fig. 3).

To adjust for potential confounding due to gestational age, gestational age was included as an independent variable in multiple linear regression analyses evaluating the association between accreta and the statistically significant parameters (fractal analysis and standard deviation of pixel intensity). The dependent Y variable was logarithmically transformed for a regression equation of $\ln(Y)=\beta_1 x_1+B_2 x_2+c$ (x_1 = pathology (0 = normal, 1 = abnormal), x_2 = gestational age in weeks, c = constant) to achieve our regression model's assumption of normally distributed data. Q–Q plots (Fig. 4) confirmed that the residuals were normally distributed, as the Q–Q plots of the residuals approximately fit the line $y=x$, representing the quantiles of the normal distribution. In addition, lack-of-fit tests (Table 4) supported the validity of our multivariable linear regression model to explain the effect of gestational age on the pixel intensity standard deviation ($p=0.139$), fractal analysis at box size 32 ($p=0.586$), and 256 ($p=0.452$), with insufficient evidence at the $\alpha=0.05$ level to conclude that there is a lack-of-fit in this model. These assumptions of normality and linearity held true when normal and abnormal placenta were separately analyzed with Q–Q plots and lack-of-fit tests. Results indicated that gestational age was not a confounder for the associations between accreta and the three most statistically significant variables (standard deviation of pixel intensity, fractal analysis at box size 32, and 256) between normal and abnormal placenta, with positive correlations between the presence of accreta and these variables remaining after adjustment for gestational age ($p<0.05$) (Table 5). Moreover, the effect of gestational age was to weakly attenuate the apparent effect of accreta on these most statistically significant variables, as the inclusion of gestational age in the regression model increased the estimate of the association (regression coefficient) between accreta and these variables by less than 10%. For stratified analysis, the data was analyzed separately by trimester, and the difference in fractal

values persisted when there was no statistically significant difference in gestational age overall ($p=0.59$) or looking only at third trimester ($p=0.74$) (Table 6). However, statistically significant differences (Table 6) were found between second and third trimester placentas for coefficient of variation ($p=0.003$) and HOG ($p<0.001$).

Discussion

Our study found statistically significant differences between normal and abnormal groups for the standard deviation of pixel intensity ($p=0.023$) and fractal analysis at every box size up to 256, suggesting potential applications of these variables in diagnosing PAS. In fractal analysis, the fractal scaling factor is not always known ahead of time. Therefore, by changing box sizes, one can typically find an optimized box size that reveals the scaling factor. In our case, it appears that a larger box size (such as 256) gives us better delineation of the fractal dimension of the placenta. In other words, the fractal dimensions of placenta tissues with different pathologies are not significantly differentiable until seen from a global perspective. PAS was associated with a higher standard deviation of pixel intensity (3.7 compared to 2.5 in the normal group) obtained from histogram analysis, which is consistent with the heterogeneous signal intensity associated with PAS [21, 22]. Predictive value of the standard deviation of signal intensity and fractal analysis may further be increased if used in conjunction with other imaging findings such as lower uterine bulging and dark intraplacental T2 bands, as considering all of the imaging findings together is important in the diagnosis of PAS [23].

The relatively high variability of the pixel intensity standard deviation among the abnormal and normal groups (s.d. of 2.8 and 1.8 respectively) may limit the predictive value of this variable in diagnosis. This wide distribution of values may be explained in part by the small sample size and the fact that the entire placenta was analyzed rather than suspicious appearing areas. Future work could analyze abnormal appearing areas or higher risk areas such as adjacent to the C-section scar, as it is believed that the pathophysiology of

Fig. 4 Normal quantile–quantile (Q–Q) plots plotting the quantiles of ▶ the standard normal distribution (indicated by the line $y=x$) versus the quantiles of the residuals of our multivariable linear regression model when the dependent variable Y is LN(sigma) (**a**), LN(df32) (**b**), and LN(df256) (**c**)

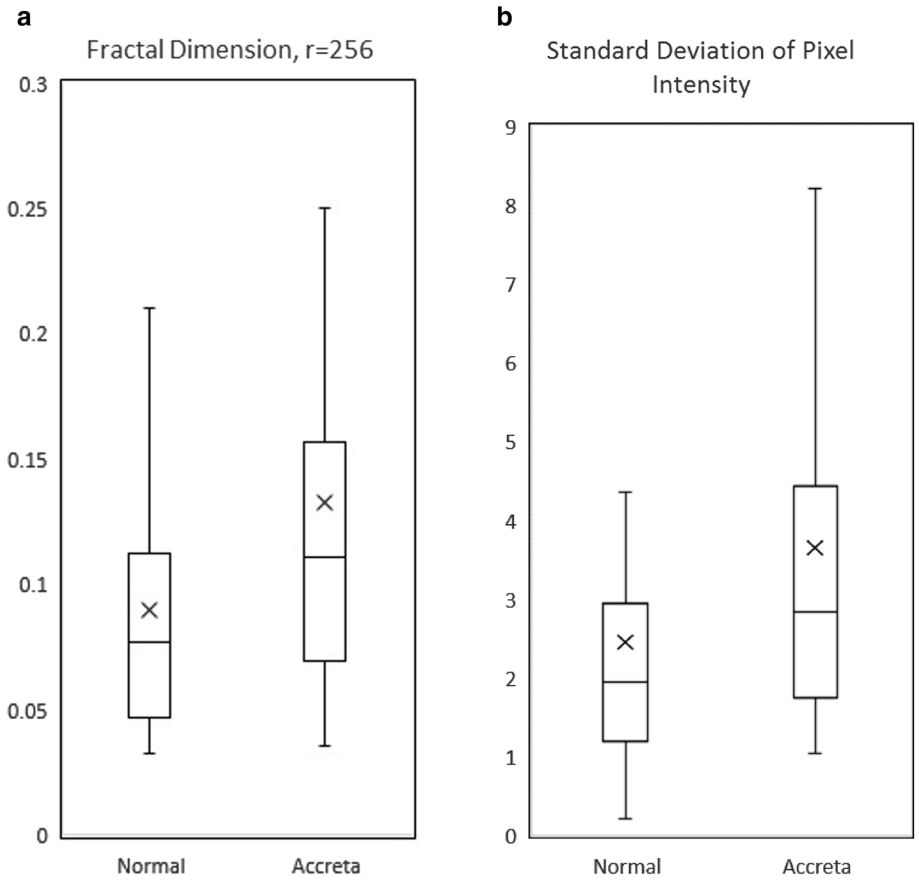

Fig. 3 Box and whisker plots for the most statistically significant variables, fractal analysis at box size 256 (**a**) and standard deviation of pixel intensity (**b**). *X* indicates the mean

a

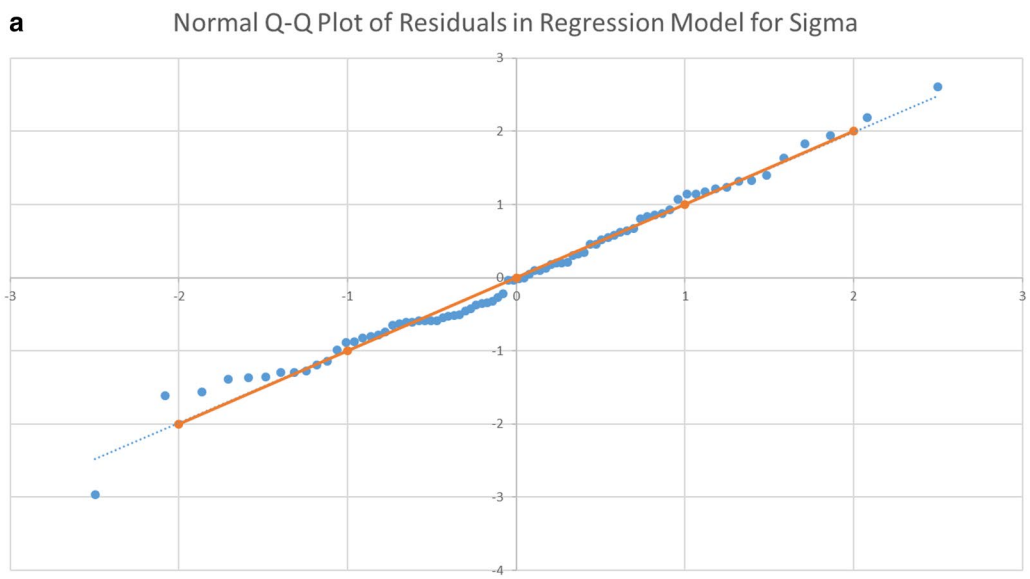
Normal Q-Q Plot of Residuals in Regression Model for Sigma

b

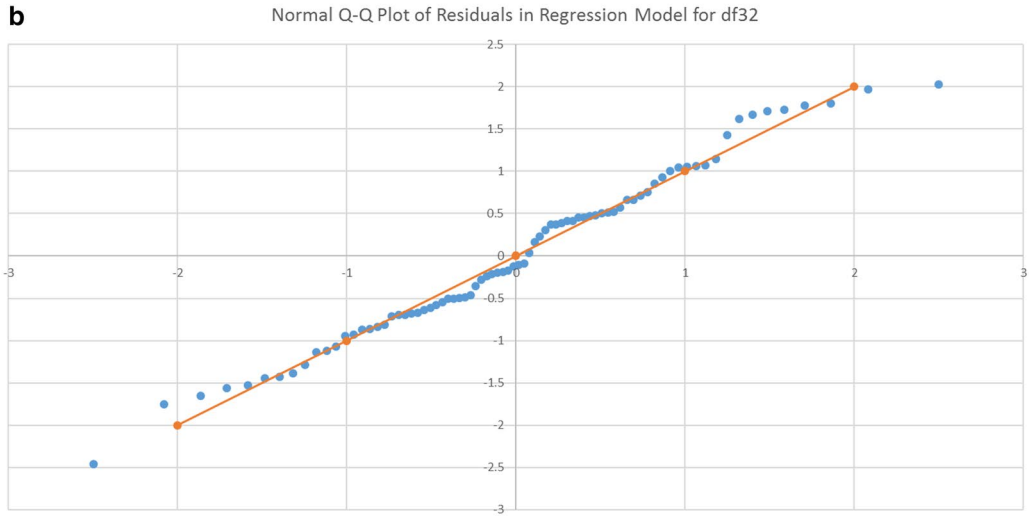
Normal Q-Q Plot of Residuals in Regression Model for df32

c

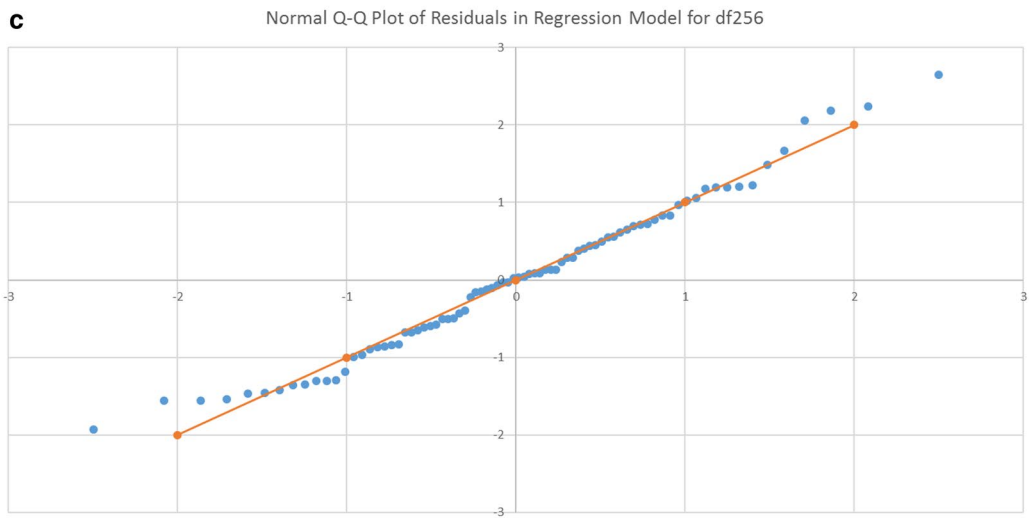
Normal Q-Q Plot of Residuals in Regression Model for df256

Table 4 Results of lack-of-fit tests for the three most statistically significant variables at $\alpha = 0.05$

Variable	DF (lack-of-fit)	DF (pure error)	*F*-value	*p*-value
Sigma	34	43	1.42	0.139
df32	34	43	0.93	0.586
df256	34	43	1.04	0.452

H_o: there is no lack-of-fit in the relationship assumed in the model. H_A: the relationship assumed in the model does not fit the data

$p > 0.05$ indicates not enough evidence to conclude that there is a lack-of-fit in this multivariable regression model

Table 5 Summary of multiple regression analyses of pathology on dependent variables with adjustment of gestational age (GA) as confounder

Dependent variable	β coefficient ± SE	*p*-value
LN(σ*)		
Without adjustment		
Pathology (0, 1)	0.410 ± 0.157	0.0109
Adjusted by GA		
Pathology (0, 1)	0.435 ± 0.152	0.0052
Gestational age (weeks)	−0.0348 ± 0.0130	0.0090
LN(df32)		
Without adjustment		
Pathology (0, 1)	0.400 ± .154	0.0111
Adjusted by GA		
Pathology (0, 1)	0.404 ± .155	0.0111
Gestational age (weeks)	−0.00455 ± .0133	0.7326
LN(df256)		
Without adjustment		
Pathology (0, 1)	0.339 ± .134	0.0137
Adjusted by GA		
Pathology (0, 1)	0.360 ± 0.130	0.0069
Gestational age (weeks)	−0.0291 ± 0.0111	0.0105

Table only displays the three variables with the most statistically significant differences between abnormal and normal pathology at α-level of .05. Pathology: 0 = normal; 1 = abnormal. *σ refers to sigma, the standard deviation of signal intensity

PAS is due to failure of normal decidualization in the area of a uterine scar [4].

In the third trimester, calcifications and vascular lakes can increase the placental heterogeneity compared to the second trimester [24], which may further confound data. Although no correlation was found between the statistically significant texture analysis variables and gestational age, heterogeneity associated with gestational age was detected with algorithms such as coefficient of variation, or HOG, indicating that each algorithm has a different sensitivity for detecting gestational age related heterogeneity. The underlying mechanism for such sensitivity difference is not known and may deserve additional investigation. As different texture analysis algorithms analyze different features, it is difficult to know prospectively which features may be detected with each variable.

Although percreta was associated with a higher number of prior C-sections compared to normal and accreta, we found no statistically significant difference in number of prior C-sections when abnormal placenta as a collective was compared to normal placenta. This may be secondary to selection bias, as patients who underwent MRI studies tended to have prior C-sections rather than representing the entire population of pregnant patients.

There are limited studies on quantitative analysis of the placenta. A study by Lim et al. calculated the volume of the intraplacental bands to compare and categorize the degree of abnormal placentation. This study suggested a higher overall volume of low signal intensity placental bands was associated with PAS [25].

A texture analysis study on heterogeneity of breast cancer on MRI by Kim et al. determined that tumors that showed more entropy, corresponding to increased heterogeneity, on T2 weighted images corresponded to decreased recurrence free survival [26]. Another study by Tiwari et al. on differentiating radiation necrosis from recurrent glioblastoma determined that computerized texture descriptors provided an accurate quantitative distinction of subtle architectural details that were not readily appreciable on original MR sequences. In this study, a histogram of gradient analysis was the most important image feature in their analysis suggesting that there was an inherent orientation difference between the two cohorts that can be detected. Additional texture descriptors that showed promise in this study were the inverse difference moment and Laws features that capture local intensity homogeneity, edges and gradients to distinguish heterogeneity between the cohorts in their study [20].

There are several limitations to our study. First, there were a relatively limited number of cases for analysis. Despite this, statistically significant results were obtained that validate the association of these variables with PAS. Second, the relative lack of increta and percreta cases limited comparison between degrees of placental invasion. Third, diagnosis using histopathology findings as the reference standard may not always be reliable, as sampling errors can occur, since the entire placenta is not able to be sampled and typically occurs from only a few areas. Fourth, it is unclear whether the maturation process is uniform or affected in abnormal placenta. Finally, the influence of different parameters such as scanner type, and other differences in imaging acquisition on texture analysis remains to be investigated.

In the future, comparison between different degrees of PAS (accreta, increta, percreta) could be performed with a larger sample size. In addition, analyzing data that controls

Table 6 Stratification by trimester for the three variables with the most statistical significance at α-level of 0.05 for *t* tests comparing normal versus abnormal pathology

	Normal (Avg)	Accreta (Avg)	*p*-value
2nd trimester: 13–27 weeks ($n=25$)	$N=10$	$N=15$	
Gestational age	20.0	22.9	0.083
σ	3.65	4.71	0.39
df32	0.686	1.26	0.051
df256	0.118	0.154	0.18
CoefVariance	4.80	4.36	0.60
HOG	11.4	12.1	0.73
3rd Trimester: 28–41 weeks ($n=55$)	$N=24$	$N=31$	
Gestational age	32.0	32.2	0.74
σ	1.96	3.14	**0.016**
df32	0.701	0.906	0.18
df256	0.0780	0.122	**0.035**
CoefVariance	6.64	5.80	0.28
HOG	20.8	17.8	0.10
Overall: 13–41 weeks ($n=80$)	$N=34$	$N=46$	
Gestational age	28.4	29.2	0.59
σ	2.5	3.7	**0.023**
df32	0.70	1.0	**0.021**
df256	0.090	0.13	**0.011**
CoefVariance	6.1	5.3	0.21
HOG	18.1	16.0	0.19

M mean, *SD* standard deviation

p value < 0.05 considered statistically significant. Statistically significant in bold

for scan parameter variables which can affect texture analysis, including magnet strength and matrix, could be helpful in confirming utility of texture analysis. Finally, future studies can focus only on abnormal or high risk areas adjacent to the cesarean scar instead of the entire placenta which may produce more predictive results, as more homogeneous regions adjacent to abnormal appearing areas may skew the data. However we still believe that there is value to this initial study analyzing the whole placenta because once there is PAS, there is a spectrum from normal to accreta to increta to percreta in the same placental bed, with altered physiology even in areas which are not frankly invaded [4]. Comparison between normal and abnormal appearing areas of the same placenta can also be performed. The testing of additional texture features and algorithm refinement could be helpful, and deep learning could also be investigated as a diagnostic adjunct.

In conclusion, our study showed statistically significant differences between normal and abnormal groups for the standard deviation of pixel intensity and fractal analysis, which suggest a potential role of these texture analysis tools in helping to diagnose PAS. These preliminary results require validation on a larger scale, and further research might focus on the application of texture analysis to differentiate between different grades of PAS once a larger sample size is obtained. Optimizing algorithms for quantitative heterogeneity analysis and controlling for confounding variables may further help to abate the subjectivity that is associated with assessing the heterogeneity of the placenta.

Acknowledgements The authors acknowledge Dr. Kruti P. Maniar, MD for assistance with clarification of pathological criteria in diagnosis of placenta accreta spectrum, and CCTS support for statistical analysis assistance (Grant Number UL1TR002003).

Compliance with ethical statement

Conflict of interest The authors declare that they have no conflict of interest.

IRB statement This study was approved by the IRB of the two main test sites, University of Illinois at Chicago and Northwestern.

References

1. Jauniaux E, Ayres-de-Campos D (2018) FIGO consensus guidelines on placenta accreta spectrum disorders: Introduction. International Journal of Gynecology & Obstetrics 140 (3):261-264. https://doi.org/10.1002/ijgo.12406
2. Warshak CR, Eskander R, Hull AD, Scioscia AL, Mattrey RF, Benirschke K, Resnik R (2006) Accuracy of ultrasonography and magnetic resonance imaging in the diagnosis of placenta accreta.

Obstet Gynecol 108 (3 Pt 1):573-581. https://doi.org/10.1097/01.aog.0000233155.62906.6d
3. Belfort MA, Medicine PCSoMF (2010) Placenta accreta. Am J Obstet Gynecol 203 (5):430-439. https://doi.org/10.1016/j.ajog.2010.09.013
4. Jauniaux E, Collins S, Burton GJ (2018) Placenta accreta spectrum: pathophysiology and evidence-based anatomy for prenatal ultrasound imaging. Am J Obstet Gynecol 218 (1):75-87. https://doi.org/10.1016/j.ajog.2017.05.067
5. Einerson BD, Rodriguez CE, Kennedy AM, Woodward PJ, Donnelly MA, Silver RM (2018) Magnetic resonance imaging is often misleading when used as an adjunct to ultrasound in the management of placenta accreta spectrum disorders. Am J Obstet Gynecol 218 (6):618.e611-618.e617. https://doi.org/10.1016/j.ajog.2018.03.013
6. Budorick NE, Figueroa R, Vizcarra M, Shin J (2017) Another look at ultrasound and magnetic resonance imaging for diagnosis of placenta accreta. J Matern Fetal Neonatal Med:1-6. https://doi.org/10.1080/14767058.2016.1252744
7. D'Antonio F, Iacovella C, Palacios-Jaraquemada J, Bruno CH, Manzoli L, Bhide A (2014) Prenatal identification of invasive placentation using magnetic resonance imaging: systematic review and meta-analysis. Ultrasound Obstet Gynecol 44 (1):8-16. https://doi.org/10.1002/uog.13327
8. Matsubara S, Takahashi H, Takei Y (2018) Magnetic resonance imaging for diagnosis of placenta accreta spectrum disorders: still useful for real-world practice. Am J Obstet Gynecol 219 (3):312-313. https://doi.org/10.1016/j.ajog.2018.04.058
9. Mar WA, Berggruen S, Atueyi U, Sekhon S, Garzon SA, Knuttinen MG, McGahan JP (2015) Ultrasound imaging of placenta accreta with MR correlation. Ultrasound Q 31 (1):23-33. https://doi.org/10.1097/ruq.0000000000000127
10. Jauniaux E, Chantraine F, Silver RM, Langhoff-Roos J (2018) FIGO consensus guidelines on placenta accreta spectrum disorders: Epidemiology. Int J Gynaecol Obstet 140 (3):265-273. https://doi.org/10.1002/ijgo.12407
11. Lubner MG, Smith AD, Sandrasegaran K, Sahani DV, Pickhardt PJ (2017) CT Texture Analysis: Definitions, Applications, Biologic Correlates, and Challenges. Radiographics 37 (5):1483-1503. https://doi.org/10.1148/rg.2017170056
12. Modzelewski R, Janvresse E, de la Rue T, Vera P (2012) Comparison of heterogeneity quantification algorithms for brain SPECT perfusion images. EJNMMI Res 2 (1):40. https://doi.org/10.1186/2191-219x-2-40
13. Skogen K, Schulz A, Dormagen JB, Ganeshan B, Helseth E, Server A (2016) Diagnostic performance of texture analysis on MRI in grading cerebral gliomas. Eur J Radiol 85 (4):824-829. https://doi.org/10.1016/j.ejrad.2016.01.013
14. Herlidou-Même S, Constans JM, Carsin B, Olivie D, Eliat PA, Nadal-Desbarats L, Gondry C, Le Rumeur E, Idy-Peretti I, de Certaines JD (2003) MRI texture analysis on texture test objects, normal brain and intracranial tumors. Magn Reson Imaging 21 (9):989-993
15. Kassner A, Thornhill RE (2010) Texture analysis: a review of neurologic MR imaging applications. AJNR Am J Neuroradiol 31 (5):809-816. https://doi.org/10.3174/ajnr.a2061
16. Zhang Y (2012) MRI texture analysis in multiple sclerosis. Int J Biomed Imaging 2012:762804. https://doi.org/10.1155/2012/762804
17. Kotu LP, Engan K, Skretting K, Måløy F, Orn S, Woie L, Eftestøl T (2013) Probability mapping of scarred myocardium using texture and intensity features in CMR images. Biomed Eng Online 12:91. https://doi.org/10.1186/1475-925x-12-91
18. Herlidou S, Rolland Y, Bansard JY, Le Rumeur E, de Certaines JD (1999) Comparison of automated and visual texture analysis in MRI: characterization of normal and diseased skeletal muscle. Magn Reson Imaging 17 (9):1393-1397
19. Alpert K, Kogan A, Parrish T, Marcus D, Wang L (2016) The Northwestern University Neuroimaging Data Archive (NUNDA). Neuroimage 124 (Pt B):1131-1136. https://doi.org/10.1016/j.neuroimage.2015.05.060
20. Tiwari P, Prasanna P, Rogers L, Wolansky L, Badve C, Sloan A, Cohen M, Madabhushi A (2014) Texture Descriptors to distinguish Radiation Necrosis from Recurrent Brain Tumors on multi-parametric MRI. Proc SPIE 9035:90352B. https://doi.org/10.1117/12.2043969
21. Derman AY, Nikac V, Haberman S, Zelenko N, Opsha O, Flyer M (2011) MRI of placenta accreta: a new imaging perspective. AJR American journal of roentgenology 197 (6):1514-1521. https://doi.org/10.2214/AJR.10.5443
22. Teo TH, Law YM, Tay KH, Tan BS, Cheah FK (2009) Use of magnetic resonance imaging in evaluation of placental invasion. Clin Radiol 64 (5):511-516. https://doi.org/10.1016/j.crad.2009.02.003
23. Lax A, Prince MR, Mennitt KW, Schwebach JR, Budorick NE (2007) The value of specific MRI features in the evaluation of suspected placental invasion. Magn Reson Imaging 25 (1):87-93. https://doi.org/10.1016/j.mri.2006.10.007
24. Baughman WC, Corteville JE, Shah RR (2008) Placenta accreta: spectrum of US and MR imaging findings. Radiographics 28 (7):1905-1916. https://doi.org/10.1148/rg.287085060
25. Lim PS, Greenberg M, Edelson MI, Bell KA, Edmonds PR, Mackey AM (2011) Utility of ultrasound and MRI in prenatal diagnosis of placenta accreta: a pilot study. AJR American journal of roentgenology 197 (6):1506-1513. https://doi.org/10.2214/AJR.11.6858
26. Kim JH, Ko ES, Lim Y, Lee KS, Han BK, Ko EY, Hahn SY, Nam SJ (2017) Breast Cancer Heterogeneity: MR Imaging Texture Analysis and Survival Outcomes. Radiology 282 (3):665-675. https://doi.org/10.1148/radiol.2016160261